The International Design Study for the Neutrino Factory

J. Scott Berg
Brookhaven National Laboratory; PO BOX 5000; UPTON NY 11973-5000; USA
A. Blondel
University de Geneve, 24, Quai Ernest-Ansermet, 1211 Geneva 4, Suisse
A. Bross, J. Morfin
Fermi National Laboratory, P.O. Box 500, Batavia, IL 60510-5011, USA
K. Long, Jürgen Pozimski
Imperial College London; South Kensington Campus; London SW7 2AZ; UK
P. Soler
School of Physics and Astronomy, Kelvin Building, University of Glasgow, Glasgow G12 8QQ,
Scotland, UK
R. Tsenov
Department of Atomic Physics, St. Kliment Ohridski, University of Sofia, 5 James Bourchier
Boulevard, BG-1164 Sofia, Bulgaria
M. Zisman
Lawrence Berkeley National Laboratory, 1 Cyclotron Road, Berkeley, CA 94720, USA

On behalf of the IDS-NF collaboration

Mail to: jsberg@bnl.gov

1. Introduction

The phenomenon of neutrino oscillations, arguably the most significant advance in particle physics over the past decade, has been established through measurements on neutrinos and anti-neutrinos produced in the sun, by cosmic-ray interactions, in nuclear reactors, and using beams produced by high-energy particle accelerators [1]. In consequence, we know that the Standard Model is incomplete and must be extended to include neutrino mass, mixing among the three neutrino flavors, and therefore lepton-flavour non-conservation. These observations have profound implications for the ultimate theory of particle interactions and for the description of the structure and evolution of the Universe. In particular:

- Mixing among the three massive neutrinos admits the possibility that the matter-antimatter (CP) symmetry is violated via the neutrino-mixing matrix;
- If a neutrino is to be distinguished from its antineutrino counterpart it is necessary to assign a conserved "lepton number" to the neutrino. At present there is no theoretical justification for such a conserved quantum number. If lepton number is not conserved, then a neutrino is indistinguishable from an antineutrino, i.e. the neutrino is a Majorana particle; a completely new state of matter; and
- The neutrino abundance in the Universe is second only to that of the photon and so, even with a tiny mass, the neutrino may make a significant contribution to the dark matter which is known to exist. Therefore, the

neutrino may play an important role in determining the structure of the Universe.

These exciting possibilities justify an energetic and far reaching program.

2. The Neutrino Factory

In the Neutrino Factory, beams of electron and (anti-) muon-neutrinos are produced from the decay of muons circulating in a storage ring. As the muon charge-to-mass ratio is large, the neutrinos carry away a substantial fraction of the energy of the parent muon, hence, high neutrino energies can readily be achieved. Time-dilation is beneficial, allowing sufficient time to produce a pure, collimated beam. Charged-current interactions induced by "golden channel," $\nu_e \rightarrow \nu_\mu$, oscillations produce muons of charge opposite to those produced by the anti-muon neutrinos in the beam and thus a magnetized detector is required. The additional capability to investigate the "silver" ($\nu_e \rightarrow \nu_\tau$) and "platinum" ($\nu_\mu \rightarrow \nu_e$) channels makes the Neutrino Factory the ideal place to look for oscillation phenomena that are outside the standard, three-neutrino-mixing paradigm. It is thus the ideal facility to serve the precision era of neutrino oscillation measurements.

The baseline specification for the Neutrino Factory, developed within the International Design Study for the Neutrino Factory (the IDS-NF), has been optimized for the discovery of CP-invariance violation, the determination of the mass hierarchy, and the determination of θ_{13} [2]. The optimum requires two distant detectors, one at the "magic baseline," 7000–8000 km, the second at a source-detector distance in the range 2500–5000 km. The sensitivity to non-standard interactions improves as the stored-muon energy is increased, reaching a plateau at around 25 GeV [3]. A baseline stored muon energy of 25 GeV has therefore been adopted. The baseline accelerator facility provides a total of 10^{21} muon decays per year split between the two distant neutrino detectors.
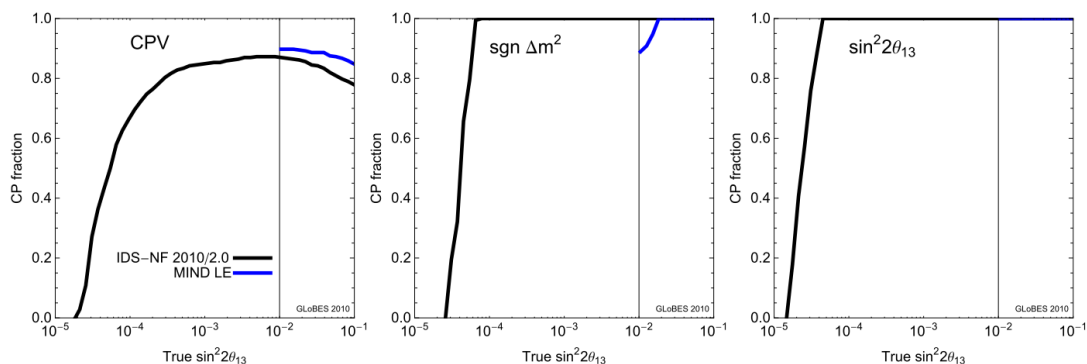
Figure 1: The discovery potential at 3σ for CP violation (left panel), the mass hierarchy (central panel), and $\sin^2 2\theta_{13}$ (right panel). The discovery reach is plotted in terms of the CP fraction as a function of $\sin^2 2\theta_{13}$. The performance of the IDS-NF baseline is shown as the black solid line. The Neutrino Factory re-optimized for large $\sin^2 2\theta_{13}$ is shown as the blue solid line.

The performance of the IDS-NF baseline in terms of the 3σ discovery reach for CP violation, the mass hierarchy, and θ_{13} is shown in Fig. 1. The discovery reach is presented in terms of the fraction of all possible values of δ (the "CP fraction") and plotted as a function of $\sin^2 2\theta_{13}$. The discovery reach of the Neutrino Factory is significantly better than realistic alternative facilities, particularly for small values of

θ_{13}. Recent results hint that θ_{13} may be large, i.e., close to the present upper bound [4]. In this case, a re-optimization of the baseline Neutrino Factory will still yield superior performance. As an example, Fig. 1 shows the performance that may be obtained with 10 GeV stored muons illuminating a detector at a distance of 2000 km from the source.

3. Layout and components of the neutrino factory accelerator complex

A schematic diagram of the Neutrino Factory accelerator facility is shown in figure 2. Muons are produced by bombarding a target with protons, resulting in the production of pions, which decay to muons. Pions and muons of both signs are captured and focused in a high-field solenoid channel designed to maximize the number of muons transported to the muon storage ring.
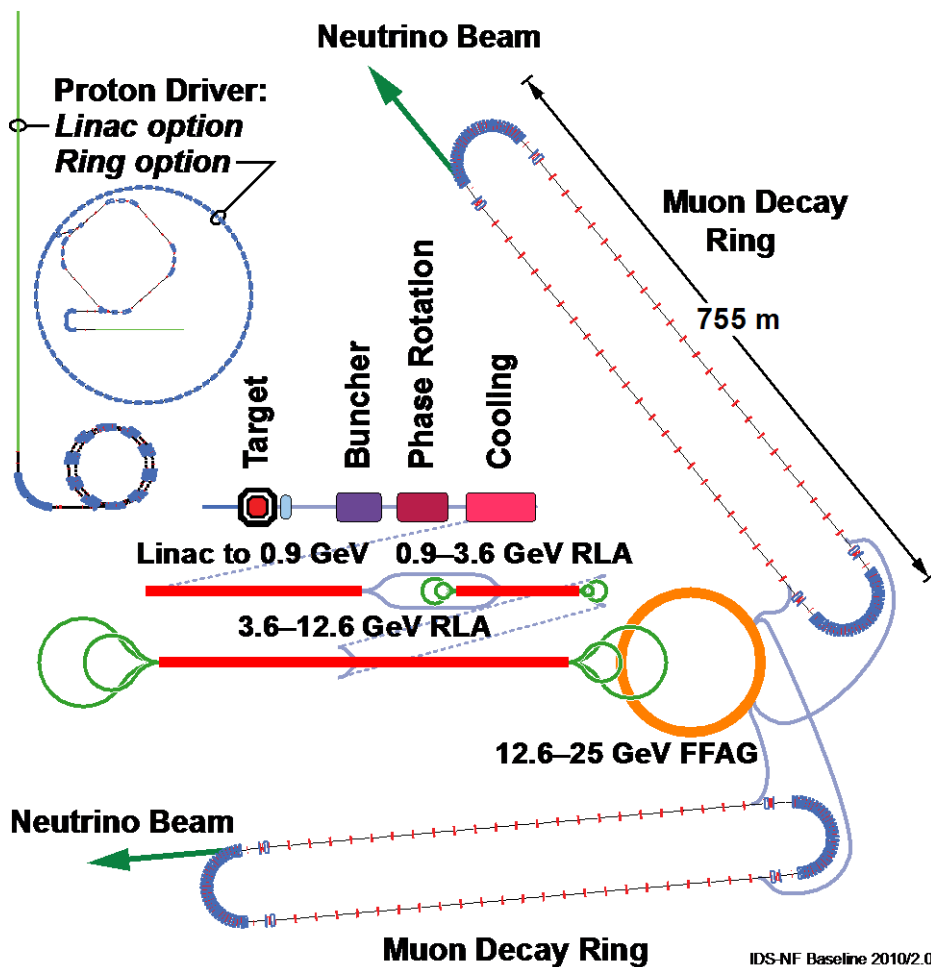
Figure 2: Layout of the IDS-NF Accelerator Systems.

The captured muons have a large energy spread and a large transverse emittance, both of which need to be reduced so that the beam can be accelerated efficiently. This is accomplished by turning a single, large-emittance bunch into a train of bunches each with a small emittance. The bunches initially have different energies spanning the range that the muons had before bunching. Phase rotation is therefore employed to give all the bunches the same mean energy and a reasonable energy spread. The transverse emittance of the bunch train is then reduced using ionization cooling.

Table 1: Parameters characterizing the muon beam produced by the accelerator facility. Muon decays are a total for all signs and detector baselines.

Parameter	Value
Muon total energy [GeV]	25
Production straight muon decays in 10^7 s	10^{21}
Maximum RMS angular divergence of muons in production straight	$0.1/\gamma$
Distance to intermediate baseline detector [km]	3000–5000
Distance to long baseline detector [km]	7000–8000

After the beam has a more reasonable emittance, it is accelerated to the final energy. To keep the efficiency of acceleration high, different acceleration schemes are used in different energy ranges. The first stage of acceleration is performed using a linac because the large transverse emittance and the variation of velocity with energy make it impractical to recirculate the low-energy beam through the cavities. The linac is followed by two recirculating linear accelerators, in each of which the beam makes multiple passes through the accelerating structures. The final stage of acceleration is performed using a linear non-scaling fixed-field alternating-gradient accelerator, which allows many more passes through the cavities.

Finally the beam is injected into two racetrack-shaped decay rings, the straight sections of which are pointed at the two distant detectors. The rings have very long straight sections to ensure that a large fraction of the muons are moving toward the detector when they decay.

3.1 Proton driver

At the start of the accelerator chain, a proton driver capable of delivering an average power of 4 MW is required. Several boundary conditions define the proton beam parameters necessary to produce the desired number of muons in the storage rings of the Neutrino Factory (see table 2). The proton-beam energy must be in the multi-GeV range in order to maximize the pion production. In addition, the Neutrino Factory requires a particular time structure consisting of 3 very short bunches separated by 120 μs. The short bunch length of 1–3 ns rms is dictated by the efficiency of the muon-beam capture and the bunch separation is constrained by beam loading in the downstream muon accelerator and the recovery time of the mercury-jet target.

Table 2: Parameters characterizing the proton beam parameters.

Parameter	Value
Proton beam energy [GeV]	5–15
Average beam power on target [MW]	4
Repetition rate [Hz]	50
Pulse duration [ns]	1–3
Bunches per 50 Hz cycle	3
Bunch separation [μs]	120

In order to achieve such short bunches, a dedicated bunch compression scenario needs to be designed carefully in order to deal with very strong space-charge forces.

Several proton driver schemes fulfilling these requirements have been proposed (see Fig. 2).

In the CERN Neutrino Factory scenario [5], which would be based on the proposed 5-GeV high-power version of the Superconducting Proton Linac (SPL) [6] and be able to deliver 10^{14} protons at a repetition rate of 50 Hz, the chopped beam from the SPL would be injected into an isochronous accumulator ring in which 120 ns long bunches are formed without the need for an RF system. The beam parameters after accumulation are obtained as a compromise between the competing requirements of minimizing the heating of the injection foil, maximizing the aperture, and adequate compensation of the space-charge forces. The beam parameters are set to allow for RF phase-rotation in the downstream compressor ring. The size of the two rings is determined by the requirement that successive bunches must arrive at the correct location in the compressor ring. The compressor ring has a large phase-slip factor, which is needed for fast phase rotation. The most recent design of the SPL and more details of the CERN proton driver scenario can be found in [7, 8].

A proton driver for a Neutrino Factory situated at Fermilab [9] would be based on an upgrade of the proposed Project X linac. Fermilab is currently designing a high intensity proton source that will deliver beam at 3 GeV and at 8 GeV and is designed such that it can be upgraded to deliver the full beam power (4 MW at 8 GeV) required for the Neutrino Factory. Just as in the CERN scheme, additional accumulator and compressor rings will be needed to provide the correct time structure. At injection into the accumulation ring there will be a stripping system, foil or laser based, to convert the H^- ions to protons. The front-end of Project X will have a programmable chopper so that beam will be injected into three RF buckets in the accumulation ring. After injection is complete, the RF bucket voltage will be increased to shorten the bunches. The accumulated protons will then be transferred to a separate bunch-shortening (compressor) ring. Bunch rotation will be used to achieve the final bunch length (2 ns). The three bunches will be extracted with the proper spacing (120 μs). The accumulation, bunch shortening, and targeting will be done at 50 Hz, as required for the Neutrino Factory. Project X will be located within the Tevatron ring at Fermilab.

A Neutrino Factory sited at the Rutherford Appleton Laboratory (RAL) [10] would be served by a proton driver based on an upgrade to the ISIS pulsed-proton source. A common proton driver for the spallation neutron source and the Neutrino Factory is proposed in the framework of the ongoing ISIS megawatt-upgrade program. In such a scenario, the proton drivers for both facilities would share the same source, chopper, linac, accumulator, and acceleration up to 3.2 GeV. After extraction, a number of bunches would be sent directly to the neutron-spallation target while three others would be injected into a second RCS where, after acceleration to somewhere between 6.4 GeV and 10.3 GeV followed by bunch compression, the beam would be extracted towards the Neutrino Factory pion-production target. For the ISIS megawatt upgrade to be compatible with the Neutrino Factory, an 800 MeV H^- linac has been designed, candidate lattices for the 3.2 GeV booster RCS have been identified, and preliminary parameters for the final RCS ring have been proposed.

3.2 Target

The proton beam will be brought into collision with a target, producing pions that decay into muons. Since a solid target is likely to be damaged by a proton beam of the

intensities that are required, a liquid-mercury-jet target has been chosen as the baseline. For the high proton-beam energies under consideration, a target material with high atomic number is preferred.

The target must operate in a high magnetic field to maximize the capture of the pions, which are emitted with a large transverse momentum. Extensive studies of the target have been performed to find the optimal proton-beam energy and target-station geometry [2]. These parameters have determined the specification of the proton beam energy and emittance. The mercury jet must have sufficient velocity for the mercury target to be reformed between proton beam pulses. The resulting parameters for the jet are given in Table 3, and a diagram of the target region is shown in Fig. 3.

The biggest challenge in the design of the target is to achieve the high magnetic fields required in a region in which the radiation-dose is very high. The large magnetic field is reached using a 14 T superconducting coil outside a 6 T copper insert. A series of superconducting magnets downstream from the target/beam crossing serves to reduce the field, thereby reducing the beam divergence and transporting the beam to the muon front end. There must be sufficient shielding in front of the superconducting magnets to keep the cryogenic loads manageable and to prevent the coils from quenching from the instantaneous energy deposition. A revision to the IDS-NF baseline target station geometry is being prepared in which additional shielding is introduced at the expense of larger solenoids. The result of a recent study of the revised shielding is compared to the baseline in Fig. 4.

Table 3: Parameters of the mercury jet target.

Parameter	Value
Jet diameter [mm]	8
Jet velocity [m/s]	20
Jet/solenoid axis angle [mrad]	96
Proton beam/solenoid axis angle [mrad]	96
Proton beam/jet angle [mrad]	27
Solenoid field at target/jet crossing [T]	20
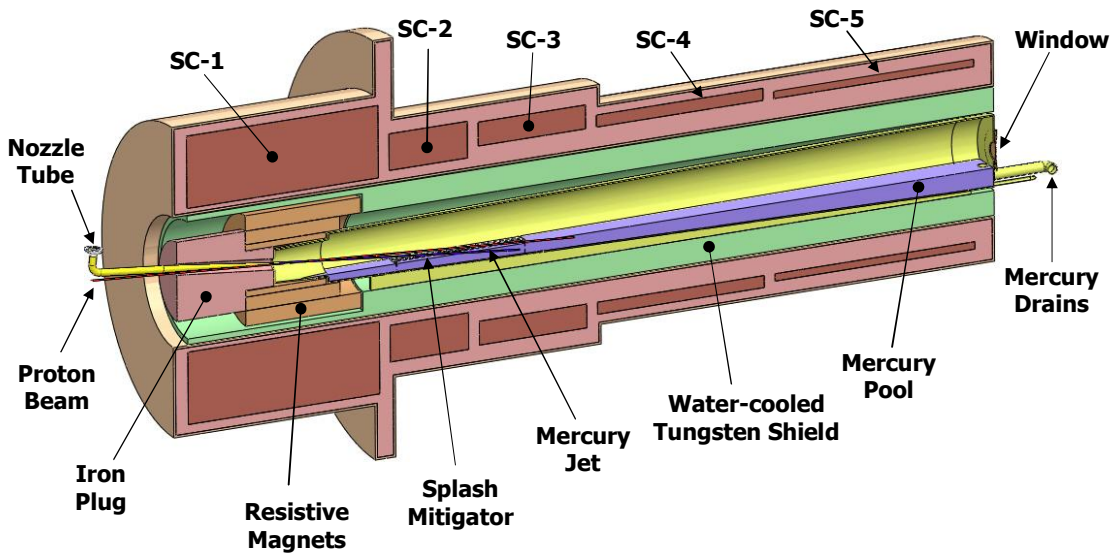
Figure 3: Cross-section of target region as envisioned in the IDR, showing the outer superconducting coils (SC-*n*), inner resistive solenoids, shielding, and portions of the mercury handling system.
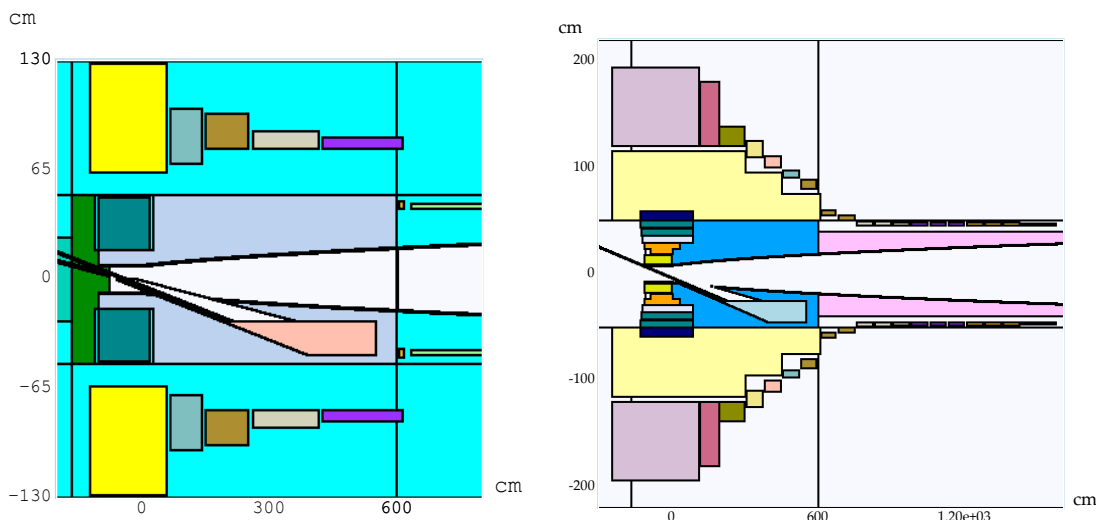
Figure 4: Target geometry from the IDS-NF (left), and a recent version of the improved target geometry (right). Note the differing scales (magnets corresponding to the downstream magnets in the right-hand figure are not shown in the left-hand figure). The inner radius of the solenoids has increased from 65 cm to 120 cm, and additional shielding has been added in the region between the inner warm and outer superconducting coils.

3.3 Muon Front-end

The Neutrino Factory muon front-end consists of a pion decay channel and longitudinal drift, followed by an adiabatic buncher, phase-rotation system, and ionization-cooling channel. It is designed to optimize the number of muons that can be transmitted through the downstream accelerator complex. The present design is based on the lattice presented in the Neutrino Factory Study 2A report [11] and subsequently developed in the ISS [12] with several modifications: the taper from the target solenoid has been adjusted; the solenoid-field strength in the drift, buncher, and phase rotation sections has been reduced from 1.75 T to 1.5 T; the whole system has been shortened; and the thickness of the lithium-hydride absorbers in the cooling section has been increased. These changes result in the same muon-capture performance in a shorter bunch train, reducing requirements on some systems downstream of the muon front-end.

Downstream of the target solenoid, the magnetic field is adiabatically reduced from 20 T to 1.5 T over a distance of 15 m to capture a secondary-pion beam with a large energy spread. As the initial proton bunch and subsequently the pion bunch is relatively short in time, the pions and their daughter muons develop a position-energy correlation in the decay channel as required for the following sections of the muon front-end. The drift channel is followed by a buncher section that uses RF cavities to form the muon beam into a train of bunches and a phase-energy rotating section that decelerates the leading high-energy bunches and accelerates the late, low-energy bunches, so that each bunch has the same mean energy.

Buncher

The IDS-NF baseline design delivers a bunch train that is less than 80 m long, a significant improvement over the ISS-design which delivered a 120 m long bunch train containing the same number of muons. A shorter bunch train will help to ease the

challenging kicker requirements for the muon FFAG and decay rings, and may allow the decay rings to be made shorter. For the present design, to capture particles around a reference momentum of $p_0 = 233$ MeV/c, with the intent of capturing muons from an initial kinetic energy range of 50 MeV to 400 MeV, the buncher length is 31.5 m. With these parameters, the RF cavities decrease in frequency from 320 MHz to 230 MHz over the length of the buncher. The initial geometry for the placement of the RF cavities uses $0.4 - 0.5$ m long cavities placed within 0.75 m long cells. The 1.5 T solenoid focusing of the decay region is continued through the buncher and the rotator section that follows. The linear ramp of cavity frequency that is required theoretically is approximated by a sequence of RF cavities that decrease in frequency along the 33 m beam transport allotted to the buncher. The number of different RF frequencies is limited to a manageable 13 and the linear ramp in gradient is approximated by the placement and gradient of the cavities in the buncher. Table 4 shows a summary of the RF cavities that are needed in the buncher, rotator, and cooling sections.

Table 4: Summary of front-end RF requirements.

	Length [m]	Number of cavities	Frequencies [MHz]	Number of frequencies	E_{peak} [MV/m]	P_{peak}
Buncher	33	37	319.6–233.6	13	4 to 7.5	1-3.5 MW/freq.
Rotator	42	56	230.2–202.3	15	12	2.5 MW / cav.
Cooler	75	100	201.25	1	15	4 MW / cav.
Total	**150**	**193**	**319.6–201.25**	**29**		**562 MW**

Rotator

In the rotator section, the RF bunch-spacing between the reference particles in each bunch is shifted away from the integer and phased such that the high-energy reference particle is stationary and the low-energy one is uniformly accelerated to arrive at the same energy as the first reference particle at the end of the rotator. This is accomplished using an RF gradient of 12 MV/m in 0.5 m long RF cavities within 0.75 m long cells (Fig. 5). The RF frequency decreases from 230.2 MHz to 202.3 MHz in steps by grouping adjacent sets of cavities into the same RF frequency. The 42-m-long RF rotator then contains 56 RF cavities grouped into 15 frequencies. At the end of the rotator, the RF frequency reaches the RF frequency of the ionization cooling channel (201.25 MHz). The average momentum at the rotator is 230 MeV/c.

Cooler

The baseline cooling-channel design consists of a sequence of identical 1.5 m long cells (Fig. 6). Each cell contains two, 0.5-m-long RF cavities, with 1.1 cm thick lithium hydride (LiH) discs at the ends of each cavity (4 per cell), and a 0.25 m spacing between cavities. The LiH discs provide the energy-loss material for ionization cooling. The cells contain two solenoid coils with opposite polarity, which produce an approximately sinusoidal variation of the magnetic field in the channel with a peak value on-axis of 2.8 T, providing transverse focusing with $\beta_\perp = 0.8$ m.

Two independently-developed codes have been used for tracking simulations of the muon front-end by the Monte Carlo method: ICOOL version 3.20; and G4beamline version 2.06. Both codes use semi-analytic procedures to compute electromagnetic

fields. Good agreement is shown in the muon yield from the two codes (see figure 7). The input beam for both simulations has been generated using MARS 15.07. The effect of the cooling can be measured by counting the number of simulated particles that fall within a reference acceptance that approximates the expected acceptance of the downstream accelerator. Using the output from our reoptimized buncher and rotator, we have tracked particles through the cooling channel, and obtain, within the reference acceptances, 0.19 muon per 8 GeV incident proton.
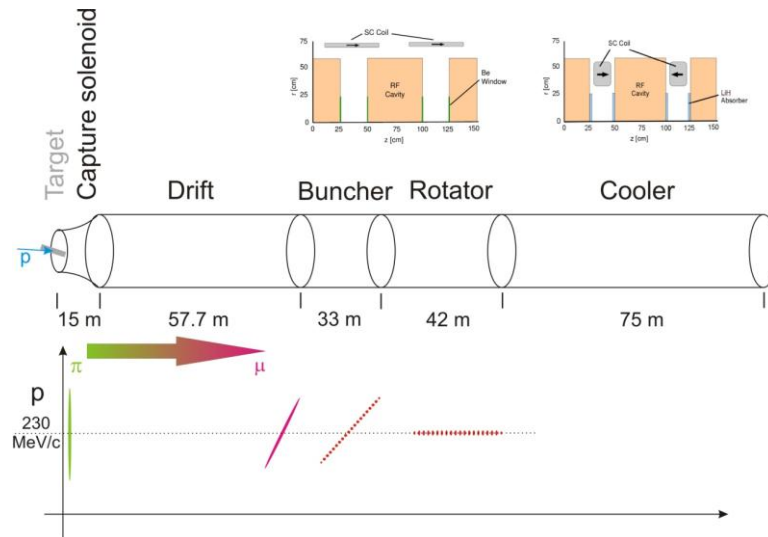
Figure 5: Schematic overview of the muon front end. The lattice design of the Buncher, Rotator and Cooler are shown in the top row, while the bottom row shows the development of the particle burst into a bunch train within the front end.
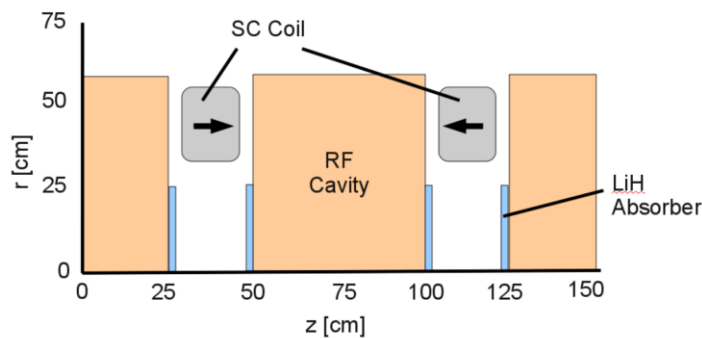
Figure 6: Schematic diagram of one cell of the ionization cooling lattice.

The performance of the bunching and phase rotation channel, along with the subsequent cooling channel, is displayed in figure 7, which shows, as a function of the distance down the channel, the number of muons within a reference acceptance. The phase rotation increases the number of "accepted" muons by a factor of four. A critical feature of the muon production, collection, bunching, and phase rotation systems is that together they produce bunches of both signs (μ^+ and μ^-) at roughly equal intensities. This occurs because the focusing systems are solenoids, which focus both signs, and the RF systems have stable acceleration for both signs, separated by a phase difference of π. The Neutrino Factory muon front-end captures a substantial proportion of the muons

produced by the Neutrino Factory target. Longitudinal capture is achieved using a buncher and energy-time phase-rotation system, while transverse capture is achieved using a high-field solenoid adiabatically tapered to 1.5 T and is enhanced by ionization cooling. Overall, the muon front-end increases the capture rate of muons in the nominal accelerator acceptance by a factor 10.
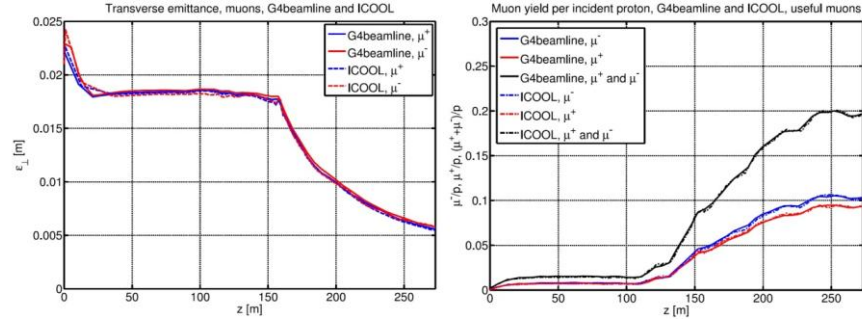
Figure 7: Performance of the bunching and cooling channel as a function of distance along the channel simulated using the ICOOL and the G4beamline codes. Left: The evolution of transverse emittance (computed over all bunches). Right: The evolution of the number of muons within a reference acceptance. The cooling section starts at $s = 155$ m, where the rms transverse emittance is 0.018 m and 0.08 μ per proton are in the reference acceptance.

Front end RF

The requirements for the normal-conducting RF cavities in the muon front-end are summarized in Table 4. The cavities are 50 cm long with peak field gradients in the range 4 MV/m to 15 MV/m, with the highest voltage required for the 201 MHz cavities. Empirical evidence suggests that magnetic fields overlapping RF cavities, as present in the muon front-end, may induce breakdown in the cavities [13, 14]. Simulations of the performance of the muon front-end using a reduced field have shown that only if the achievable RF gradient falls dramatically below the nominal value, is there a significant effect on muon transmission. In order to mitigate this technical risk, several alternative lattices have been developed (see reference [2]).

Front end magnets

The 1.5 T solenoids for buncher and rotator must accommodate the beam pipe, with a 30 cm radius and must also accommodate RF cavities with radii of 60 cm. This can be achieved using coils with an inner radius of 68 cm and a conductor radial thickness of 4 cm, so that the cavities fit entirely within the coils. A coil length of 50 cm spaced at 75 cm intervals leaves a gap of 25 cm between the coils, matching the periodicity of the cooling channel and enabling access for room temperature services such as vacuum and RF power feeds. The required current for these coils is 47.5 A/mm^2 to give a total current of 0.95 MA-turns. The coils are therefore large enough to accommodate the beam pipe, RF and diagnostics, and shielding. A smaller radius could be used in the first 60 m, where there is no RF. The 135 m transport requires 180 such magnets. The cooling system requires strong alternating-sign coils that are placed between RF cavities. These coils (see Table 5) produce an on-axis solenoid field that varies from +2.8 T to −2.8 T over a 1.5 m period, following an approximately sinusoidal dependence. Maximum fields in the cooling cell volume are 5 T near the coil surfaces; 100 such coils are needed in an 80 m cooling system.

Table 5: Summary of front-end magnet requirements.

	Length [m]	Inner radius [m]	Radial thickness [m]	Current density [A/ mm^2]	Number
Initial transport	0.5	0.68	0.04	47.5	180
Cooling channel	0.15	0.35	0.15	±107	100

There are significant particle losses along the beam line and these will result in a large energy deposition in the superconducting magnets and other equipment. Two main risks have been identified: energy deposition by all particles may cause superconducting equipment to quench; and energy deposition by hadrons and other particles may activate equipment, preventing hands-on maintenance. In currently operating accelerators, uncontrolled hadronic losses must be less than ≈1 W/m to allow "hands-on" maintenance without additional time, distance, or shielding constraints. Magnets are expected to quench with beam losses above a few tens of W/cm^3. Several schemes are envisaged to control the beam losses and reduce them below these values. Particles with a high momentum, outside of the acceptance of the front-end, can be removed using a pair of chicanes, where dispersion is induced in the beam by means of tilted solenoids and high-momentum particles are passed onto a beam dump. The chicane would be followed by a proton absorber removing low momentum protons taking advantage of the different stopping distance of protons compared with other particles in material. Additionally, particles with transverse amplitude outside of the acceptance of the front-end may be removed using transverse collimators.

3.4 Acceleration

The muon beam must be accelerated from a total energy of 244 MeV to 25 GeV. This is made more challenging by the large transverse and longitudinal emittances of the beam. Acceleration will be performed in four stages with three different types of accelerators, each chosen to give the best efficiency for its energy range. Throughout the system, 201.25 MHz superconducting RF cavities will be used to accelerate the beam. Tables 6 and 7 give the parameters for the acceleration system, while Figure 8 shows a conceptual layout of the acceleration systems.

Table 6: Overall parameters for the acceleration system.

Parameter	Value
Initial total energy [MeV]	244
Final total energy [GeV]	25
Normalized transverse acceptance [mm]	30
Normalized longitudinal acceptance [mm]	150
RF frequency [MHz]	201.25
Maximum RF gradient [MV/m]	17

Table 7: Parameters for acceleration stages

Type	Linac	RLA	RLA	FFAG
Min. total energy [GeV]	0.244	0.9	3.6	12.6
Max. total energy [GeV]	0.9	3.6	12.6	25
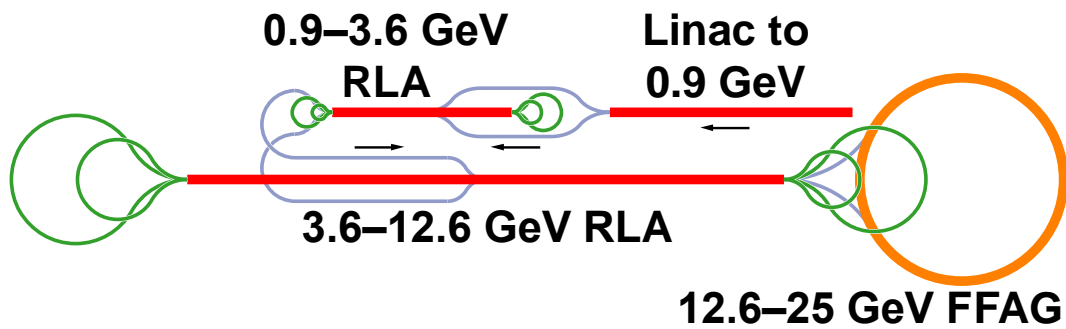
Figure 8: Structure of the acceleration systems.

Linac

A rough measure of the efficiency of acceleration is the number of passes that the beam makes through an RF cavity. However, due to the beam's large emittance and energy spread, as well as its significant velocity variation with energy, recirculating the beam through the RF cavities at the lowest energies would be impractical, resulting in excessive beam loss and emittance growth. Thus, acceleration begins with a linac. The linac consists of three types of cells (shown in Fig. 9), which increase in length and add more RF voltage per cell as the beam accelerates and the transverse geometric emittance decreases. Acceleration starts far off-crest to capture the large longitudinal emittance, then the RF phase moves approximately linearly with length to the crest by the end of the linac.

To improve the transverse acceptance of the linac, we are in the process of re-designing the linac to use only the first two types of cells, with larger aperture cavities for the later cells having a gradient of 15 MV/m.

RLAs

Once the muon beam has reached a sufficiently high energy (0.9 GeV), two recirculating linear accelerators (RLAs) are used. The first RLA raises the beam energy to 3.6 GeV, the second takes the beam energy to 12.6 GeV. Both RLAs include a number of arcs, each designed to return muons of a particular energy to the linac at the appropriate phase, allowing the beam to make 4.5 passes through the accelerating structures. A dog-bone geometry has been chosen for the RLAs since it gives better beam separation at the switchyard for a given energy gain in the linac, allowing a larger number of passes through the linac. The beam is injected into the center of the linac to reduce the RF phase mismatch resulting from the velocity variation of the beam as it is accelerated.

The switchyard and arc crossings in the RLAs are particularly challenging due to the large beam emittances. To simplify these sections, provide additional space between beam lines, and simplify the matching between the linac and the arcs, the designs presented in the IDR will be updated. Chicanes injecting into the RLA linacs will be re-designed to add more space. The arcs will be re-designed to match into the linacs better: the ordering of magnets will change (defocusing quadrupoles at the ends), and the cell lengths will be made comparable to the linac cell lengths. The arc crossings will be re-designed to avoid changing the vertical height unnecessarily. The linac quadrupole strengths will also be adjusted to use a beta-beat to improve the matching into the arcs.
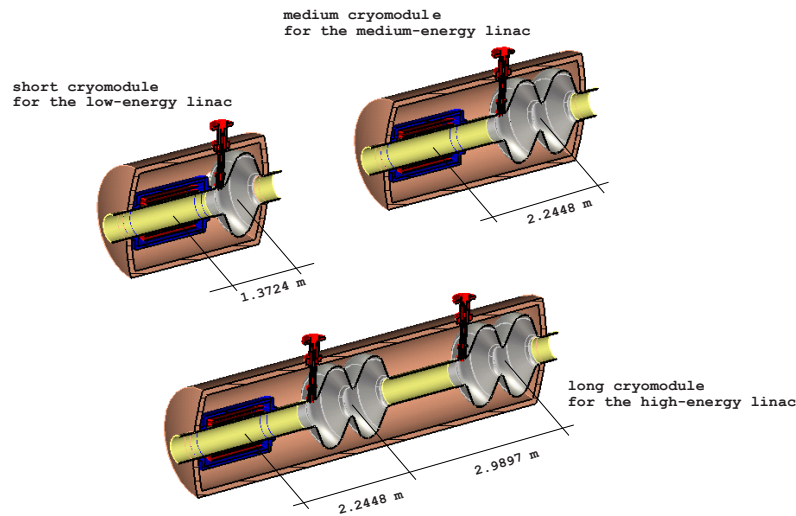
Figure 9: Different modules in the linac.

FFAG

    The final acceleration stage will use a non-scaling fixed-field alternating-gradient (FFAG) accelerator. This machine has a single arc with a very wide energy acceptance, allowing the beam to accelerate over its full range in the same arc. This avoids the switchyard in the RLAs which limits the number of passes through the cavities. The lattice consists of nearly identical triplet cells, with RF cavities in most of the long drifts. Table 8 summarizes the important parameters of the ring.

Table 8: Parameters of the FFAG ring.

Parameter	Value	
Cells	64	
Circumference [m]	667	
RF Cavities	48	
On-crest energy gain per cavity [MeV]	25.5	
Quadrupoles	D	F
Length [m]	2.3	1.1
Aperture radius [mm]	137	163
Maximum field [T]	6.1	4.3

Table 9: Parameters for kicker magnets in the FFAG. "Pattern" gives the arrangement of kickers in successive cells: − means an inward kick, + means an outward kick, and ○ means an empty drift. There are septa in the cells adjacent to the two end kickers. Each system injects or extracts both muon beam signs simultaneously.

Parameter	Injection	Extraction
Kickers	2	4
Pattern	−○−	++○○++
Kicker field	0.089 T	0.067 T
Septum field	0.92 T	1.76 T
Kicker/septum length	4.4 m	4.4 m

The most challenging parts of the FFAG lattice are the insertions for injection and extraction. The required magnet aperture is large, the kicker rise/fall time must be short and the beam energy is relatively high. In addition, since three beam pulses arrive in rapid succession, there must be three separate pulse-forming networks for each kicker. The parameters of the kicker magnets are given in Table 9.

3.5 Muon Storage Rings

Intense bursts of neutrinos and anti-neutrinos are generated by the decays of the muon bunches in long straight sections in dedicated storage rings. The neutrinos are directed through the Earth to detectors at distances of between 2500 km and 5000 km and between 7000 km and 8000 km at angles to the surface of ~18° and ~36°, respectively.

Different geometries of storage rings [2] have been studied, of which the most flexible are based on race-track lattices (Fig. 10), which are built to point towards the two neutrino detectors. The return straight can be used for collimation, RF and tune control. An alternative is a triangular lattice with two production straights that can be pointed in different directions and so send neutrinos to combinations of detectors.
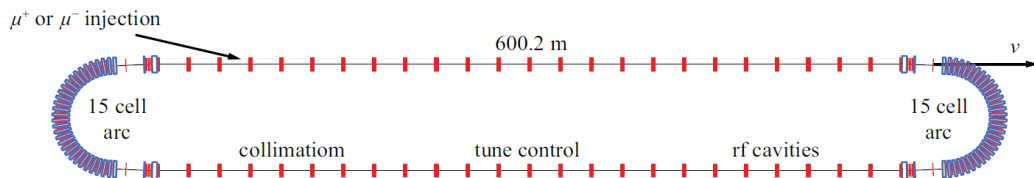
Figure 10: Race-track design for the Neutrino factory storage rings.

Based on the proton driver described above, a decay ring of 1.6 km in circumference can accommodate the equally-spaced, 250 ns long bunch trains and can allow time intervals of at least 100 ns between the neutrino bursts. The production straights for the race-track design are 600.2 m long, giving an efficiency of 37.5% and the tunnel depth for the far detector ring of this size is 444 m. To keep the neutrino beams reasonably well focused, the muon beam's rms divergence angle should not add more than about 10% to the natural $1/\gamma$ angle of the decay cone, implying large β–functions (~150 m) in the long production straights. Matching these β–functions to values of ~14 m in the arcs (chosen to reduce the size of the beam and maximize transmission) is accomplished by dedicated matching sections at the end of each straight, which also eliminate the high dispersion in the arcs. A detailed description of the decay ring lattice can be found in [2]. Simulations of the race-track decay ring using the code Zgoubi [15] prove that the neutrino angular distribution will meet the Neutrino Factory requirements. Additional simulations showed that, assuming the predicted energy spread of the muons is achieved, the bunches in the bunch train will not merge sooner than twice the lifetime of the muons, so no RF need be installed in the decay ring.

Studies of the beam instrumentation in the decay ring—essential for the correct prediction of the expected neutrino flux at the far detector—have been performed [2]. To measure the muon divergence, systems utilizing Cherenkov radiation and optical transition radiation have been considered. The muon beam energy can be monitored by spin-polarization measurements. An efficient collimation system must be developed to

cope with the high muon-beam power along with a beam injection system able to cope with large beams with the short time-gaps between the bunch trains.

4. The neutrino detectors

The IDS-NF baseline for the Neutrino Factory includes having two Magnetized Iron Neutrino Detectors (MINDs), one with a fiducial mass of 100 kton at ~4000 km and another with a fiducial mass 50 kton at ~7500 km (the "magic baseline") [2]. The detector is optimized to carry out the detection of the "golden channel" through the wrong-sign muon signature. This strategy is more efficient for resolving degeneracies in the neutrino-oscillation formulae and provides better sensitivity than, for example, measuring the golden and the "silver" channel simultaneously.

The baseline MIND detector presented in the IDR has a cuboidal geometry with a cross-sectional area of 15×15 m^2 and length of either 63 m or 125 m, depending on the mass of the detector. The thickness of each plane of iron is 3 cm, followed by two planes of scintillator, each with a thickness of 1 cm. The three planes form a module of thickness 5 cm. The lateral resolution requirement is 1 cm, which is provided by having co-extruded scintillator bars 15 m long and 3.5 cm wide, read out using optical fibers and silicon photo-multipliers (SiPMT). A 1 T dipole field was assumed.

The simplified geometry and magnetic field were adopted to allow comparison with previous simulations. However, a more realistic octagonal geometry (14 m octagonal iron plates as shown in Fig. 11) with a toroidal field of between 1 T and 2.2 T over the whole fiducial area is now being studied. These parameters can be achieved with a 100 kA/turn current traversing the center of the MIND plates and have been shown to be feasible to manufacture.
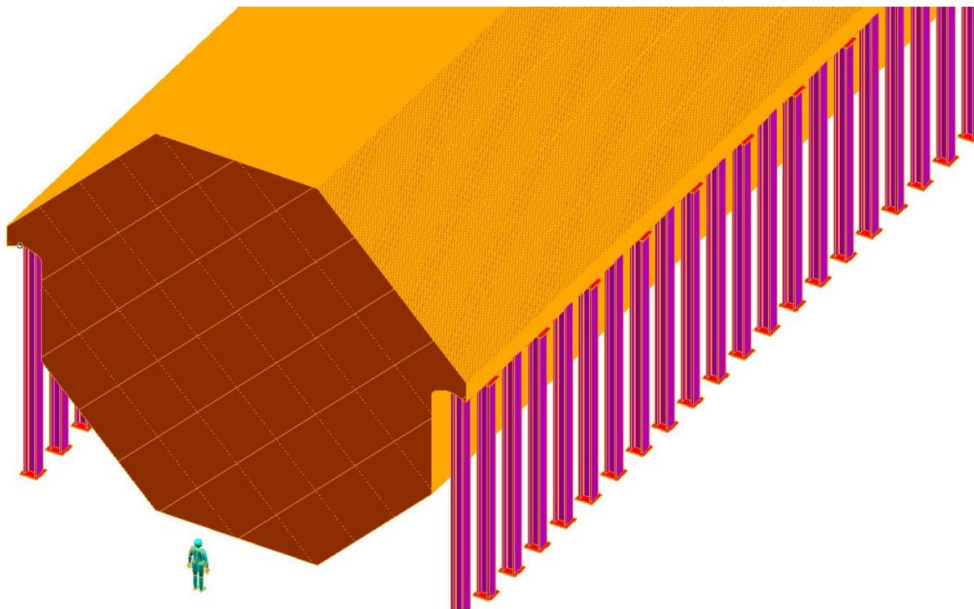
Figure 11: Schematic drawing of the Magnetized Iron Neutrino Detector (MIND).

The baseline for the Neutrino Factory includes the one or more "near" detectors located close to the end of the production straights. It is necessary to have one near detector for each of the straight sections of the storage ring at each of the two polarities,

so four near detectors designed to carry out measurements are essential for the sensitivity of the oscillation-physics program to be achieved. The near-detector measurements that are essential for the neutrino oscillation analysis include the determination of the neutrino flux through the measurement of neutrino-electron scattering and the measurement of the neutrino-beam properties that are required for the flux to be extrapolated with accuracy to the far detectors. In addition, it will be necessary to measure the charm production cross sections and the neutrino-nucleon deep inelastic, quasi-elastic, and resonant-scattering cross sections.

The intense neutrino beam delivered by the Neutrino Factory makes it possible to carry out a unique neutrino-physics program at the near detectors. This program includes fundamental electroweak and QCD physics, such as measurements of parton distribution functions as a function of Q^2 and Bjorken x, QCD sum rules, nuclear re-interaction effects, strange particle production, and a precise measurement of $\sin^2\theta_W$. The near detector must also be capable of searching for new physics, for example by detecting tau-leptons, which are particularly sensitive probes of non-standard interactions at source and at detection. Tau neutrino detection is also important in the search for sterile neutrinos.

5. The Neutrino Factory as part of the muon-physics program

The properties of the muon make it a unique tool for particle physics. In addition to the decays that provide intense, high-energy, electron neutrino beams, the great precision with which properties such as $g-2$ can be calculated using the Standard Model makes it an ideal tool in the search for new phenomena. Furthermore, the observation of charged-lepton flavor violation (cLFV) in muon decay, predicted in many models, would revolutionize current theories, while the muon's comparatively large mass and point-like nature make it an appealing candidate to provide multi-TeV lepton-antilepton collisions at a Muon Collider.

Neutrino oscillations involve processes in which lepton flavor is not conserved. Therefore, processes such as $\mu \to e\gamma$, $\mu \to eee$, and muon-to-electron conversion in the field of the nucleus ($\mu N \to eN$) will occur. Rates for such cLFV processes can be calculated in the Standard Model extended to take into account neutrino oscillations but they are minuscule (of the order of 10^{-54}) and so the observation of such processes would be a clear signal of new physics. To achieve the requisite sensitivities, intense muon beams are required and the techniques proposed for the Neutrino Factory, such as high power, pulsed proton beams with short ($\sim$10 ns) bunches, pion capture in solenoidal fields, the manipulation of muon beams of large emittance, and FFAG acceleration are of great relevance.

A Muon Collider [16] offers crucial advantages over an e^+e^- collider of the same center-of-mass energy and luminosity because the muon mass is roughly 200 times that of the electron. The large muon mass leads to a relatively low rate of synchrotron radiation, making it possible to design a circular machine in which 100% of multi-TeV $\mu^+\mu^-$ collisions occur within $\sim$0.1% of the nominal center-of-mass energy of the collider. In addition, should the Higgs boson be discovered and have the expected coupling proportional to mass, the Muon Collider could be used as a "Higgs Factory" at which detailed studies of its properties may be carried out.

A conceptual design for the Muon Collider has been proposed [17] in which the systems that make up the Neutrino Factory form the "front-end" of the Muon Collider.

Indeed, should the techniques required to realize the Neutrino Factory be demonstrated, the principal accelerator-system challenge that would remain for the Muon Collider would be the development of an ionization-cooling system that could reduce all six phase-space dimensions of the muon beams such that a luminosity in excess of 10^{34} cm^{-2} s^{-1} could be achieved. Therefore, the implementation of the Neutrino Factory is desirable to mitigate the technical risks presented by the Muon Collider.

Thus, the Neutrino Factory is the facility of choice for the study of neutrino oscillations: it has excellent discovery reach and offers the best precision on the mixing parameters, particularly in the difficult region of small θ_{13}. The ability to vary the stored-muon energy and perhaps the detector technology can provide the flexibility to respond to developments in our understanding and the discovery of new phenomena. The R&D program required to make the Neutrino Factory a reality will directly benefit the development of the Muon Collider and experiments that seek to discover cLFV. A comprehensive muon-physics program is compelling indeed.

References

1. C. Amsler et al, "Review of Particle Physics", in "Physics Letters B", 667, 1, (1008).
2. S. Choubey et al, the IDS-NF collaboration, "Interim Design Report", https://www.ids-nf.org/wiki/FrontPage/Documentation?action=AttachFile&do=get&target=IDS-NF-020-v1.0.pdf.
3. J. Kopp, M. Lindner, and T. Ota, "Discovery reach for non-standard interactions in a neutrino factory," Phys. Rev. D 76 (2007) 013001, arXiv:0702269 [hep-ph].
4. K. Abe et al, T2K Collaboration, "Indication of Electron Neutrino Appearance from an Accelerator-produced Off-axis Muon Neutrino Beam", Phys. Rev. Lett. **107**, 041801, arXiv:1106.2822 [hep-ex] (2011);
   P. Adamson et al, MINOS Collaboration, "Improved search for muon-neutrino to electron-neutrino oscillations in MINOS", Submitted to: Phys. Rev. Lett. arXiv:1108.0015 [hep-ex] (2011).
5. A. Blondel (Ed.) et al, "ECFA/CERN studies of a European neutrino factory complex", CERN-2004-002 (2004).
6. B. Autin *et al.*, "Conceptual design of the SPL, a high-power superconducting H⁻linac at CERN", CERN-2000-012 (2000).
   F. Gerigk *et al.*, "Conceptual design of the SPL II: A high-power superconducting H⁻ linac at CERN", CERN-2006-006, (2006);
   F. Gerigk *et al.*, "Layout and Machine Optimization for the SPL at CERN", CERN-ATS-2010-208, (2010).
7. M. Aiba, "Feasibility Study of Accumulator and Compressor for the 6-bunches SPL based Proton Driver", CERN-AB-2008-060, (2008).
8. R. Garoby, E. Benedetto, M. Aiba, and M. Meddahi, "Linac-based Proton Driver for a Neutrino Factory", CERN-NEUTRINO-FACTORY-NOTE-157 (2009).
9. S. D. Holmes, "Project X—Reference Design Report", Project-X-doc-776 (2010).
10. C.R. Prior, "Muon Storage Rings for the Neutrino Factory", Proceedings of the US Particle Accelerator Conference, PAC'09, Vancouver, Canada, May 2009.
    J. Pasternak, M. Aslaninejad, K. Long and J. Pozimski, "Feasibility of a

common proton driver for a neutron spallation source and a neutrino factory", Proceedings of the 23rd Particle Accelerator Conference (2010).

11. C. Albright et al, "The neutrino factory and beta beam experiments and development", physics/0411123 (2004).

12. M. Apollonio *et al.*, "Accelerator Design Concept for Future Neutrino Factories", J. Inst. P07001 (4) (2009).

13. A. Moretti *et al.*, "Effects of high solenoidal magnetic fields on rf accelerating cavities," Phys. Rev. ST Accel. Beams 8 (2005) 072001.

14. R. B. Palmer *et al.*, "RF breakdown with external magnetic fields in 201 and 805 MHz cavities," Phys. Rev. ST Accel. Beams 12 (2009) 031002.

15. F. Méot, "6D Beam Dynamics Simulations in FFAGs using the ray-tracing code ZGOUBI", ICFA Beam Dynamics Newsletter 43, *op.cit.*

16. M. M. Alsharo'a *et al.*, "Recent progress in neutrino factory and muon collider research within the muon collaboration," Phys. Rev. ST Accel. Beams 6 (2003) 081001.

17. R. B. Palmer, "Muon collider progress," in Proceedings of the 23rd Particle Accelerator Conference [473], pp. 652–656.